Numerical Modeling Efforts in Support of 3-D Environmental Variability and Acoustic Vector Field Studies

Kevin B. Smith
Code PH/Sk, Department of Physics
Naval Postgraduate School
Monterey, CA 93943
phone: (831) 917-4902 fax: (831) 656-2084 email: kbsmith@nps.edu

Award #: N0001411WX20707

LONG-TERM GOALS

The goals of this work were multi-faceted, consistent with the various efforts supported by this work. One aspect was the continued study of the effects of three-dimensional (3-D) environmental variability on propagation and the flow of energy in the acoustic field. This included modeling efforts conducted at URI to support analysis of SW06 data sets in the presence of non-linear internal waves (in collaboration with Prof. Jim Miller of URI and Prof. Mohsen Badiey of UDel). Additional modeling efforts were also expanded to include 2-D and 3-D scattering from rough ocean interfaces and other features (in collaboration with Prof. Mohsen Badiey of UDel), in partial support of data analysis of the KAM08 and KAM11 experiments. In addition, work was conducted to support the PhD (URI) research of Bob Barton (NUWC-Newport) that involved the fundamental analysis of complex vector field scattering from canonical objects (spheres and cylinders). Both theoretical and experimental work was performed and results compared for rigid spheres and cylinders, while numerical modeling was completed for elastic materials. The goal of this effort was to determine if the complex vector intensity contained additional information unique to the scattering from such objects.

OBJECTIVES

The overall objectives of this work were to study the three-dimensional response of the underwater acoustic vector field in the presence of environmental variability, and to perform fundamental analysis of the scattered complex intensity field from canonical objects.

APPROACH

A primary element of this work was the continued study of features of the 3-D acoustic vector field in the presence of environmental variability. This included extensions of the FY10 efforts with URI and UDel to explore the shallow water variability introduced by non-linear internal waves (NLIWs). The focus in FY10 was on confirming predictions of the influence of a train of wavefronts on the focusing and/or refraction of acoustic intensity. In FY11, this was expanded to investigate modal coupling features, and a variability analysis associated with ranges of geoacoustic parameters defined for this region.

Report Documentation Page

Form Approved
OMB No. 0704-0188

1. REPORT DATE	2. REPORT TYPE	3. DATES COVERED
SEP 2011		**00-00-2011 to 00-00-2011**

4. TITLE AND SUBTITLE	5a. CONTRACT NUMBER
Numerical Modeling Efforts in Support of 3-D Environmental Variability and Acoustic Vector Field Studies	5b. GRANT NUMBER
	5c. PROGRAM ELEMENT NUMBER
6. AUTHOR(S)	5d. PROJECT NUMBER
	5e. TASK NUMBER
	5f. WORK UNIT NUMBER
7. PERFORMING ORGANIZATION NAME(S) AND ADDRESS(ES) **Naval Postgraduate School,Code PH/Sk, Department of Physics,Monterey,CA,93943**	8. PERFORMING ORGANIZATION REPORT NUMBER
9. SPONSORING/MONITORING AGENCY NAME(S) AND ADDRESS(ES)	10. SPONSOR/MONITOR'S ACRONYM(S)
	11. SPONSOR/MONITOR'S REPORT NUMBER(S)

12. DISTRIBUTION/AVAILABILITY STATEMENT
Approved for public release; distribution unlimited

13. SUPPLEMENTARY NOTES

14. ABSTRACT

15. SUBJECT TERMS

16. SECURITY CLASSIFICATION OF:			17. LIMITATION OF ABSTRACT	18. NUMBER OF PAGES	19a. NAME OF RESPONSIBLE PERSON
a. REPORT **unclassified**	b. ABSTRACT **unclassified**	c. THIS PAGE **unclassified**	**Same as Report (SAR)**	**14**	

In collaboration with UDel (Prof. Mohsen Badiey), various versions of the MMPE model (Smith, 2001) were combined for the purposes of computing the influence of a 2-D rough surface on the 3-D acoustic propagation. The 2-D propagation model also included the incorporation of a 1-D dynamic surface model, allowing not only numerical predictions of the scattered field but also estimates of the associated Doppler spread. Such analysis was used to investigate observed features collected during previous experiments conducted by UDel collaborators.

For the scattering work, the previous analytical analysis of scattering from spheres was expanded to include finite element scattering from cylinders. Vector field data was collected (in-air) in the NPS anechoic chamber for a rigid cylinder (made of solid oak) for values of ka ~ 3. Model-data comparisons were then made to determine the degree to which the predicted structures in the field could be physically observed in the data.

WORK COMPLETED

The 3-D Monterey-Miami PE (MMPE) model was upgraded for a portion of this work to incorporate a 3-D environmental structure containing a train of NLIWs based on measurements made during SW06 collected by UDel. This structure was based upon a sound speed profile measured near the source location during an event where the NLIW front appeared reasonably uniform between the source and receiver at a distance of 15km. The orientation of the wave front relative to the source/receiver line was approximately 5 deg, and the analysis examined features of the predicted field at orientations from the source of 0deg, +/-2deg, and +/-4deg. Finally, results from the modeling efforts were compared to measured data.

The 2-D MMPE model was also upgraded for a portion of this work to incorporate a 1-D dynamic rough surface ocean model. The surface wave spectra was based on observations made during the KAM08 experiment. Analysis of the scattering from the rough surface was performed, computing impulse arrival structure geo-temporal correlation times over the band 11 - 21 kHz. Model-data comparisons were then performed.

The theoretical framework for computing 3-D scattering from 2-D rough surfaces was also developed and recently implemented in another 3-D version of the MMPE model. Basic surface structures such as concentric rings and single, planar surface waves were utilized to evaluate the performance of the model. The introduction of more realistic, complicated 2-D rough surface models is underway.

For the vector intensity scattering work, preliminary analysis was completed on the measured data from scattering by a rigid cylinder in an anechoic chamber, and efforts to develop a finite-element model of scattering from a general, elastic cylinder were initiated. Some model-data comparisons were performed to investigate the robustness of some features within the complex vector intensity field.

RESULTS

3-D Propagation Studies:

For the SW06 event examined in this study, a NLIW train crossed between the source and receiver almost exactly parallel to the direct-line propagation path. Surface observations suggested that the angle between the direct-line path and the NLIW front was around 5 deg. Figure 1 shows a general layout of the geometry investigated. The cross-range profile illustrated at range 0 is valid along the propagation range. The 3-D MMPE model computed solutions in Cartesian coordinates from the source location along numerous cross-ranges. This allowed the response to be examined at virtual receive array locations, including those positions parallel to the wave front and off-axis.

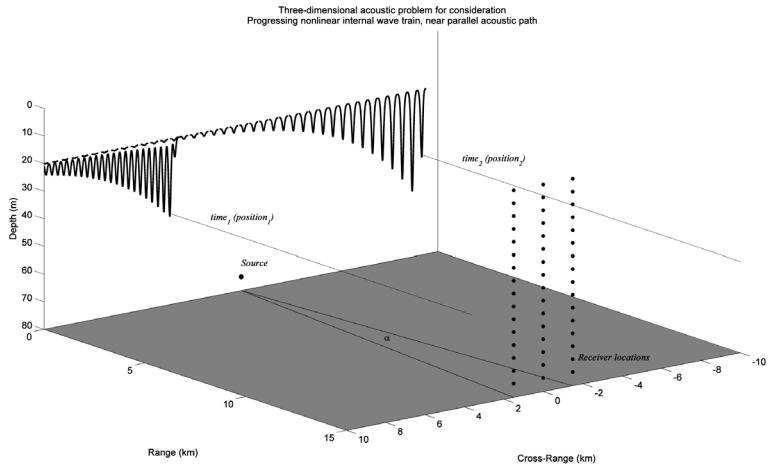

Figure 1: A general layout for the acoustic problem of interest.

Figure 2 displays results of the 3-D propagation model at 100 Hz for scenarios that highlight Lloyd's mirror type refraction as the NLIW front approaches, defocusing as the leading NLIW front sits atop the source location, and focusing between two NLIW fronts. The top panels show the sound speed profile relative to the 100 Hz acoustic source (marked by a star). The center panels show depth integrated intensity throughout the three-dimensional water column. The bottom panels show transmission loss versus depth 15 km away from the acoustic source.

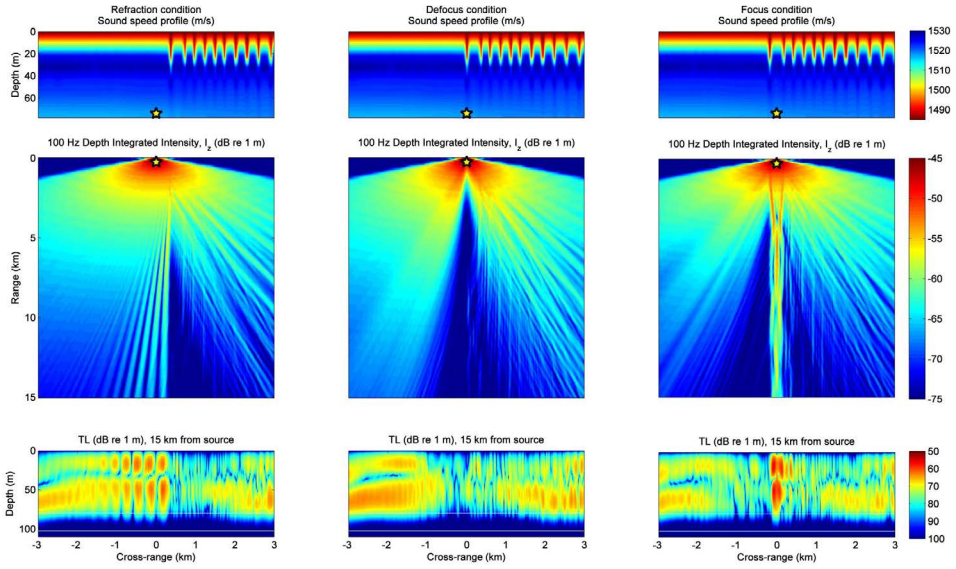

Figure 2: Three scenarios showing refraction (left), defocusing (center), and focusing (right).

In Fig. 3, the energy distribution at the receive array is displayed as the NLIW train passes by. The angle between the wave front and the source-receiver path is varied between ± 4˚ to show the large variability of acoustic receptions for very small angle variations. The panels on the left depict the NLIW marching across distance (or time). These data are normalized for each individual plot. Right-most panels show the associated distributions with the expected mean and variance annotated. Mean and variance values are referenced to the entire model data set.

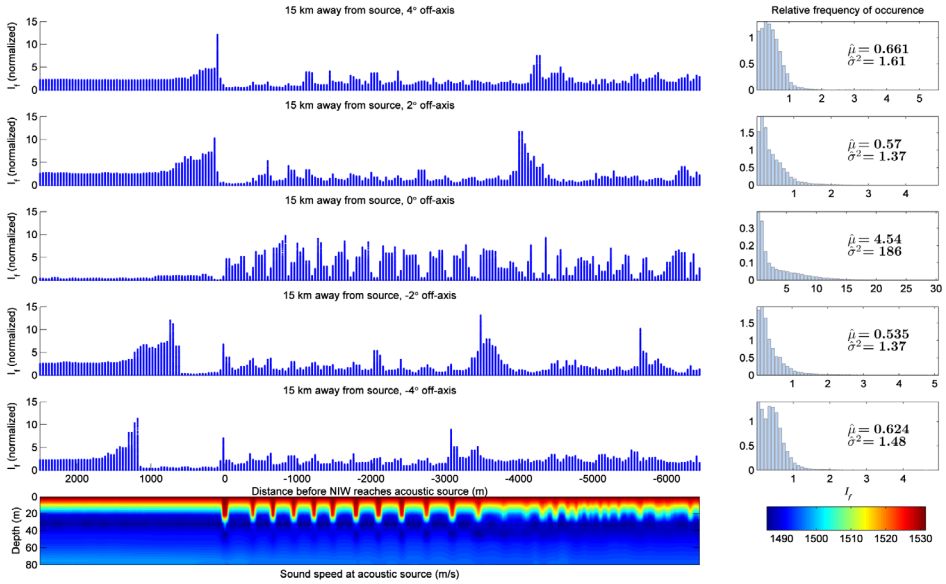

Figure 3: Energy dependence for instances where the acoustic track is near parallel to the NLIW front.

We note that the results from the parallel track indicate very little build-up in energy as the NLIW front approaches, but then large variations in level appear due to focusing and defocusing of energy. The mean value of the energy distribution is observed to be quite large. At -4 deg, however, there is a ramp-up of received energy, more consistent with the measured data. This if followed by a relatively quiet period due to the refraction of energy ahead of the leading edge of the NLIW. Once the wave train starts crossing the source location, some modest level of focusing and defocusing can still be observed, but the mean energy levels are much lower.

In Fig. 4, the structure of the field during the refraction prior to the arrival of the NLIW front is examined in more detail. In addition to the depth-integrated, broadband, normalized intensity, the solution is displayed over depth, revealing that most of the energy resides in the lower part of the water column. The lower panel also shows the modal decomposition of the field during this event.

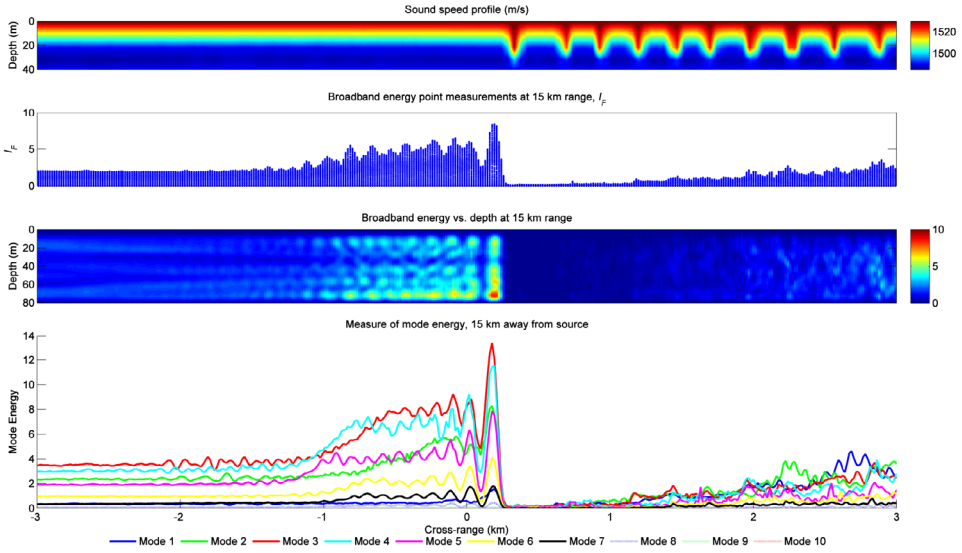

Figure 4: Energy distribution for a refraction scenario. Broadband energy measurements are shown in the center panels (as point measurements and versus depth). Modal energy distribution is shown on the bottom.

2-D Rough Surface Scattering Studies:
Figure 5 provides a schematic of the KAM08 experimental setup. Figure 6 shows a sample impulse response for a broadband signal (12.5 – 17.5 kHz) computed from the 2-D MMPE model with the rough surface scattering approach. Figure 7 then displays the results from the model compared with the KAM08 measured data at a depth of 61.5 m.

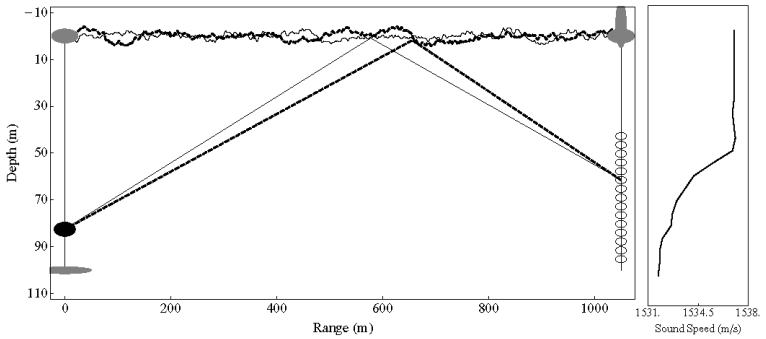

Figure 5: A schematic of the KAM08 experimental setup, including the measured sound speed profile. The solid and dotted ray paths indicate possible reflections from the respective solid and dotted surface waves.

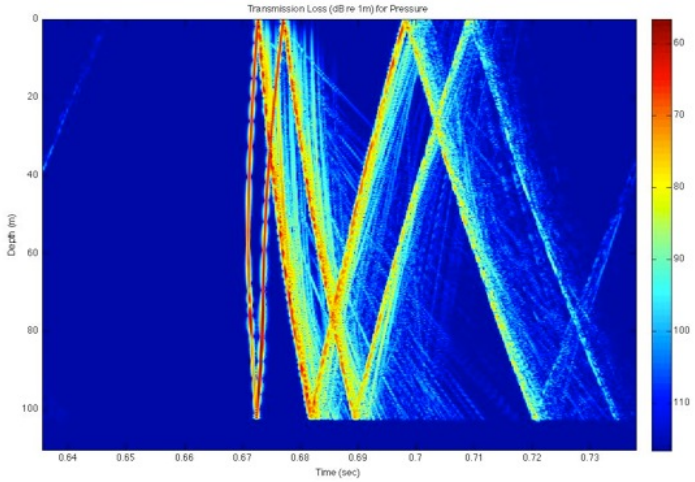

Figure 6: Broadband pulse arrival structure from 2-D MMPE after undergoing rough surface scattering.

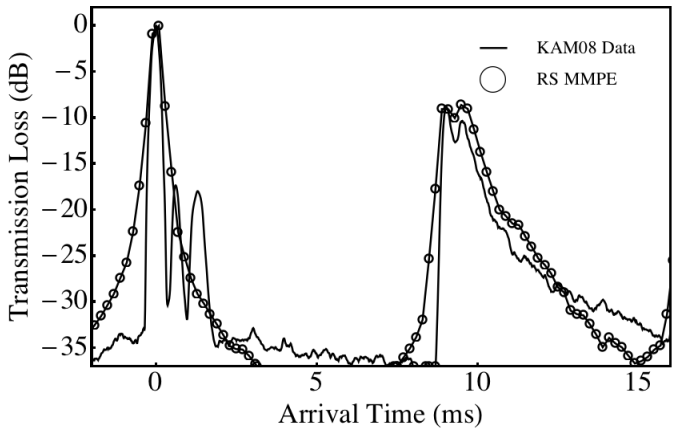

Figure 7: Comparison of model results with measured data from KAM08 experiment.

The general levels and signal decay rates in the scattered signals appear to match well. The data also exhibits some additional, low-level direct arrivals that are not accounted for in the model. These are possibly due to unknown details in the background sound speed profile or possibly source characteristics that were not included in the numerical calculations. The focus, however, was on the surface scattered structure, and that appears to be well modeled. This provides confidence in future studies to explore aspects of the dynamic surface scattering, such as the associated Doppler spread. Such studies are anticipated to occur in FY12.

3-D Rough Surface Scattering Studies:
Previous versions of MMPE that incorporated rough surface scattering were limited to 2-D calculations (with a 1-D surface defined). The approach used was based on previous work by Tappert and Nghiem-Phu (1985). In order to extend this to 3-D (with a 2-D surface defined), it was necessary to re-derive the field equations corresponding to the displaced surface field transformation in 3-D. The derivations showed that the typical 3-D MMPE model (now in cylindrical coordinates) could be utilized, based on the transformed equations

$$\frac{\partial \tilde{\psi}}{\partial r} = -ik_0\left(\tilde{T}_{op} + \tilde{V}_{op} + \tilde{U}_{op}\right)\tilde{\psi} \tag{1}$$

where the operators

$$\tilde{T}_{op} = 1 - \sqrt{1 + \frac{1}{k_0^2}\frac{\partial^2}{\partial z^2}} \quad \text{for all depths } z, \tag{2}$$

$$\tilde{V}_{op} = \begin{cases} -\dfrac{1}{2k_0^2 r^2}\dfrac{\partial^2}{\partial \phi^2} & , \quad z > \eta(r,\phi) \\ -\dfrac{1}{2k_0^2 r^2}\dfrac{\partial^2}{\partial \phi^2} + 2\dfrac{i}{k_0 r^2}\left[\dfrac{\partial^2 \eta}{\partial r \partial \phi}(z-\eta) - \dfrac{\partial \eta}{\partial r}\dfrac{\partial \eta}{\partial \phi}\right]\dfrac{\partial}{\partial \phi} & , \quad z < \eta(r,\phi) \end{cases}, \tag{3}$$

and

$$\tilde{U}_{op} = \begin{cases} U_{op}(r,z,\phi) & , \quad z > \eta(r,\phi) \\ U_{op}\left(r, -z + 2\eta(r,\phi), \phi\right) - 2\dfrac{\partial^2 \eta}{\partial r^2}(z-\eta) & , \quad z < \eta(r,\phi) \end{cases}, \tag{4}$$

where

$$U_{op}(r,z,\phi) = -\left[n(r,z,\phi) - 1\right]. \tag{5}$$

The parameter $n(r,z,\phi)$ is the 3-D index of refraction and the surface boundary is defined at depth $z = \eta(r,\phi)$. The field function is related to the usual PE field function through the transformation

$$\psi(r,z,\phi)=\begin{cases}\tilde{\psi}(r,z,\phi) & ,\quad z>\eta(r,\phi)\\ e^{-i2k_0\frac{\partial\eta}{\partial r}(z-\eta)}\tilde{\psi}(r,z,\phi) & ,\quad z<\eta(r,\phi)\end{cases}. \tag{6}$$

It may be noted that the forms of Eqs. (2) and (5) correspond to the Thomson and Chapman (1983) WAPE approximation, while the azimuthal coupling term in Eq. (3) utilizes the standard PE approximation. In cylindrical coordinates, this approximation may be considered adequate. The azimuthal coupling from the rough surface scattering is now described by the additional term in Eq. (3) for depths $z<\eta(r,\phi)$.

Figure 8 displays a sample solution from this 3-D model for a simple, concentric ring of sinusoidal surface displacements. The surface displacements were exaggerated for clarity of effect, and defined as having an amplitude of 10m with a wavelength of 200m. Figure 8(a) provides a plan-view graphic of the surface displacement, while Figure 8(b) and 8(c) display the solution in the vertical plane (for bearing $\phi=0$) and in the horizontal plane at a depth of $z=40\text{m}$, respectively. In this case, only vertical scattering occurs since there is no azimuthal variability. Figure 9 displays a similar solution for a set of planar, sinusoidal surface displacements. The effects of both vertical and azimuthal scattering are evident here.

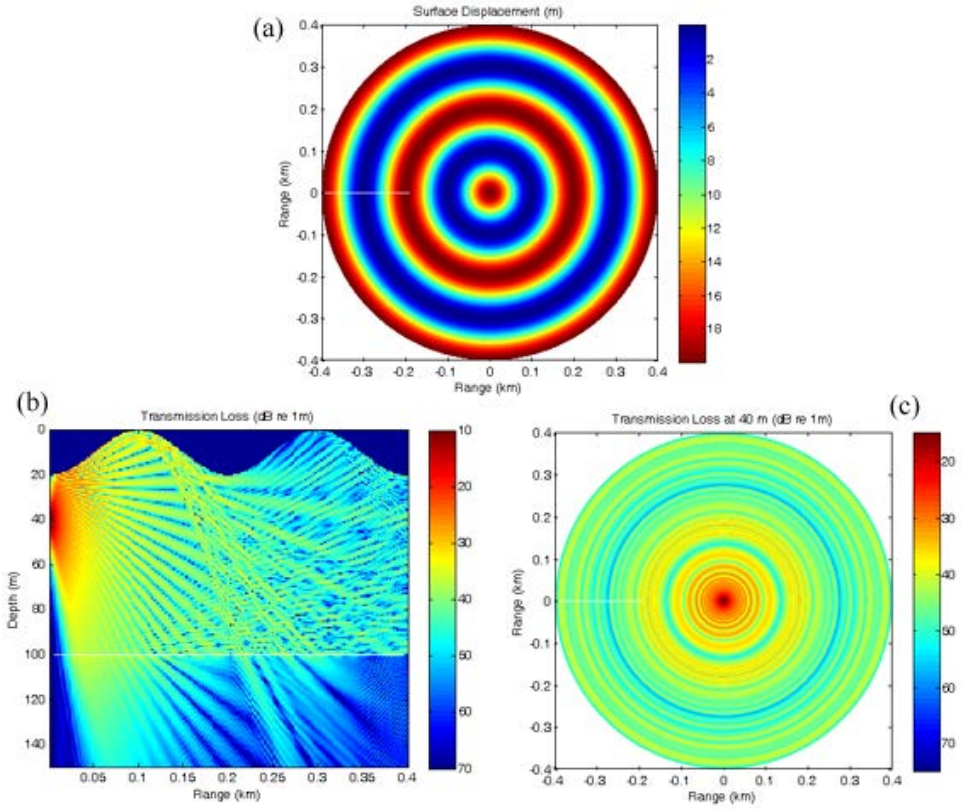

Figure 8: Sample model data with 3-D rough surface scattering model. Surface defined by concentric sinusoidal displacements, providing no azimuthal variability or scatter (scattering limited to vertical plane).

Vector Intensity Scattering Studies:
The vector intensity scattering work was a continuation of an FY10 project (funded under NUWCDIVNPT ILIR) that developed the theoretical framework for decomposing the scattered acoustic intensity field due to spherical scatterers. An experiment was conducted in the NPS anechoic chamber with a rigid (solid oak) sphere, and results were obtained using a Microflown acoustic vector sensor (in air). These results showed general agreement with features obtained from the theoretical expectations, as shown in Fig. 11.

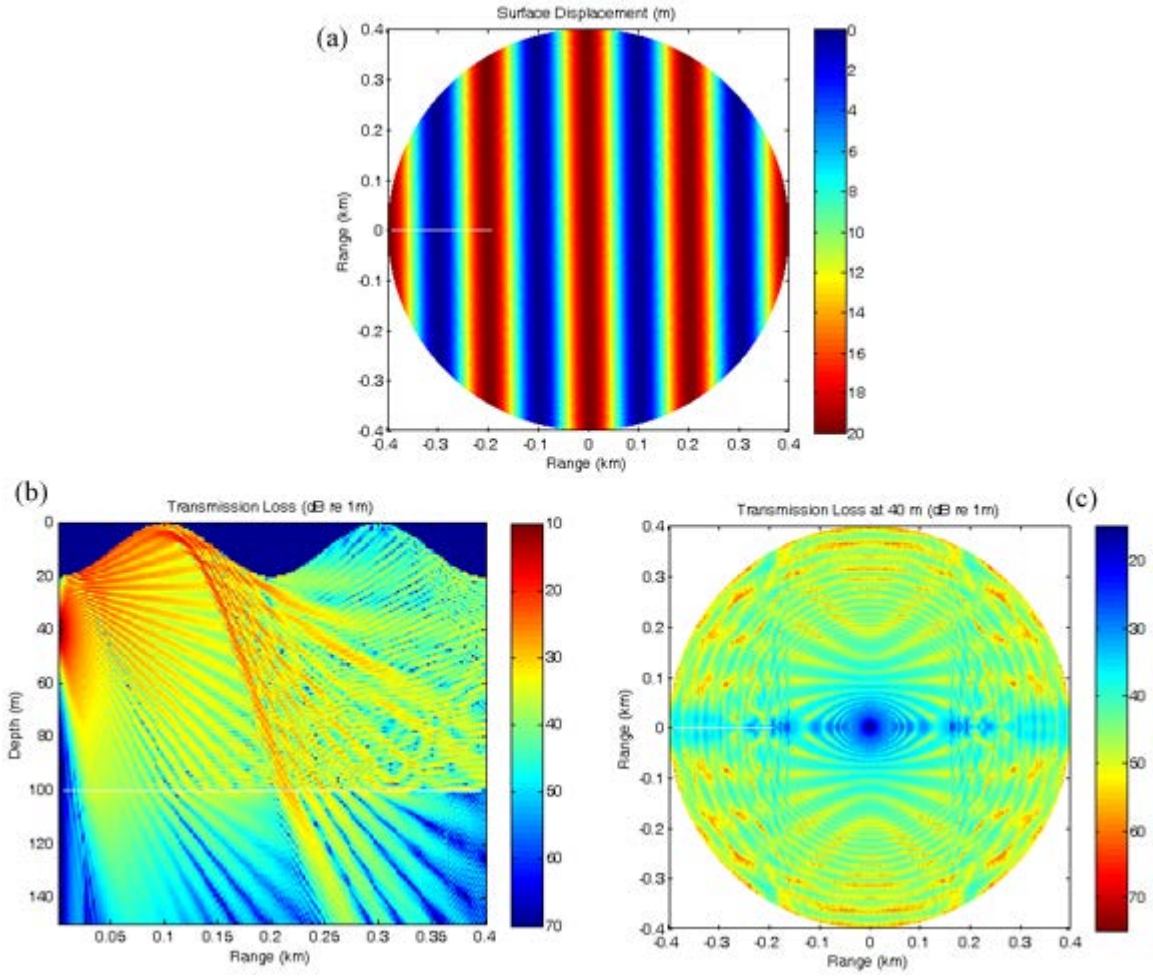

Figure 9: Sample model data with 3-D rough surface scattering model. Surface defined by planar sinusoidal displacements, providing azimuthal variability and out-of-plane scattering.

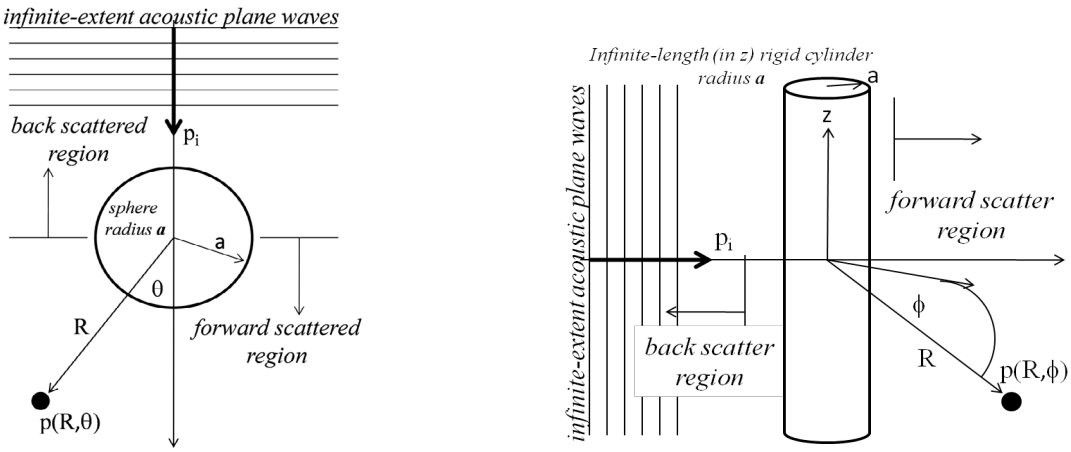

Figure 10: Geometries defining plane wave scatter from a sphere and finite cylinder.

In FY11, work was performed to develop a finite element model of the scatter from a finite cylinder. Data was again collected in the NPS anechoic chamber with a rigid (solid oak) cylinder. An example of the finite element results in provided in Fig. 12. Data was again collected in the NPS anechoic chamber with a rigid (solid oak) cylinder. The preliminary analysis of the measured data as compared with finite element results also appears to indicate that general features of the scattered complex acoustic intensity field are in agreement with predictions. Results comparing measured data to finite element results are provided in Fig. 13.

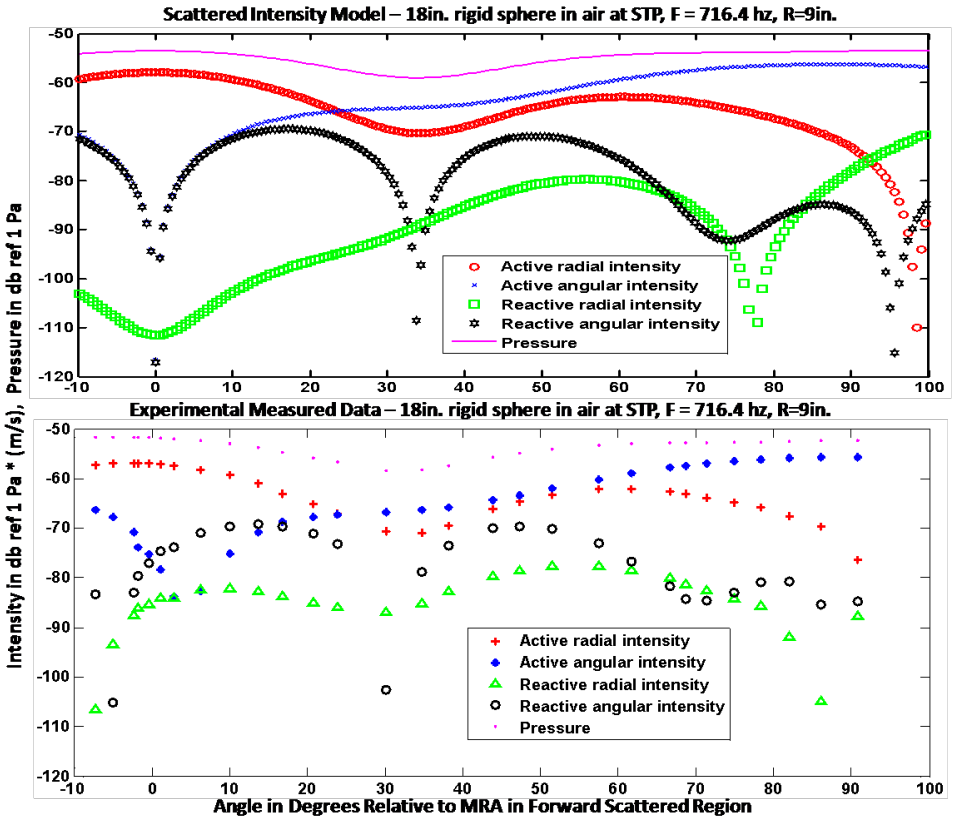

Figure 11: Model (upper panel) and measured (lower panel) data of decomposed complex intensity field in the forward scattering region of a rigid sphere.

IMPACT/APPLICATIONS

The impact of the work done on modeling 3-D propagation effects due to nonlinear internal waves and comparisons with data is to show an improved understanding of these effects and how they can generate significant fluctuations in the received signal levels.

The impact of the work done on modeling the 2-D propagation effects due to rough surface scattering is to provide a tool for future use in the development of acoustic communication algorithms and testing. The comparison with measured data was good enough to suggest that the model is capable of generating realistic structure due to rough surface scattering at these frequencies.

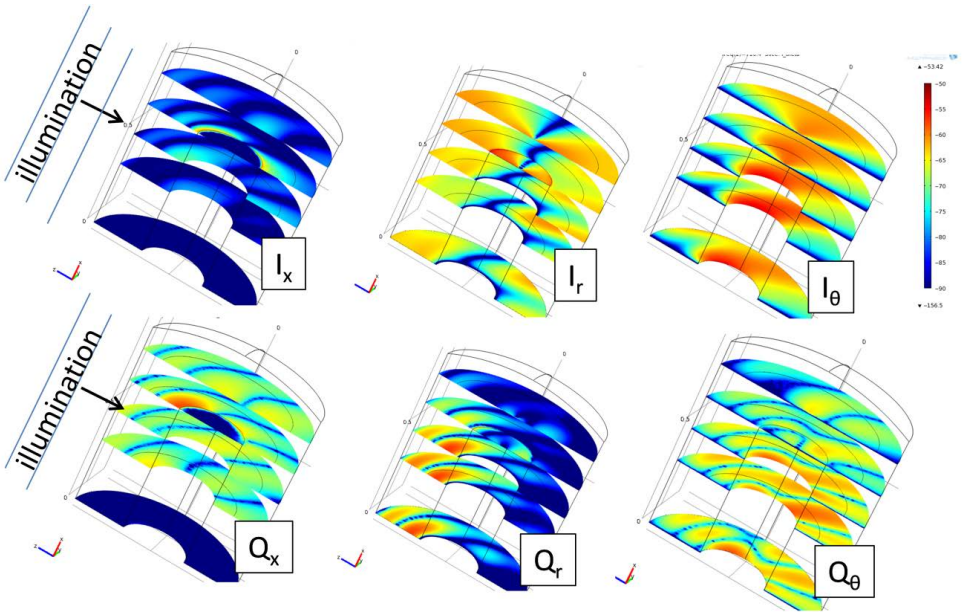

Figure 12: Finite element results of complex intensity decomposition in the forward scattering region of a rigid, finite cylinder.

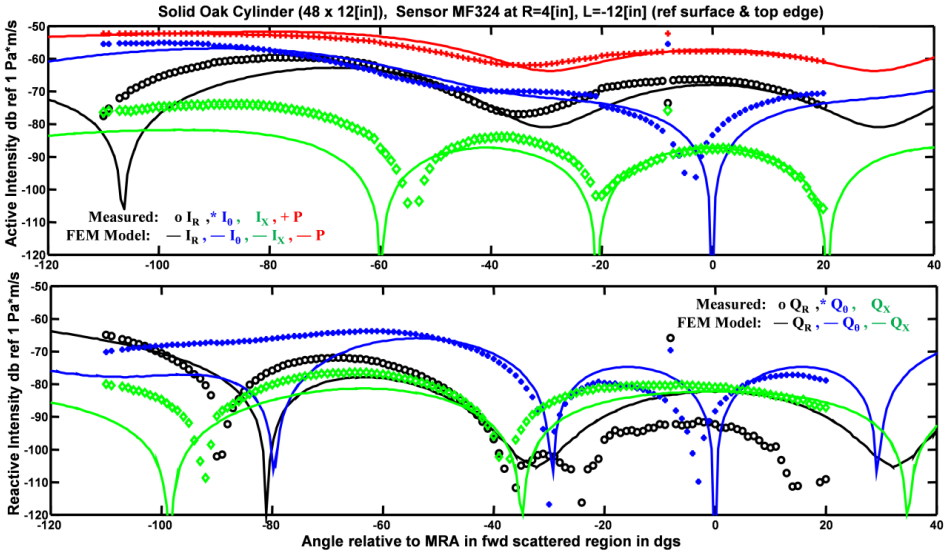

Figure 13: Model/data comparison of decomposed complex intensity field in the forward scattering region of a rigid, finite cylinder. Upper panel shows active intensity results, lower panel shows reactive intensity results.

The impact of the work done on extending the surface scattering model to 3-D is to allow researchers in future models to directly compute the 3-D, out-of-plane scattering effects of the sea surface. This could also be applied to the development of acoustic communication algorithms, or possibly be utilized to study the effects on high-frequency sonar systems.

The studies of the acoustic scattered vector field have helped provide new insight into the field structure in the presence of target scatterers. It is possible that the additional information in the scattered vector field could be utilized in classification algorithms applied to submerged targets.

RELATED PROJECTS

The rough surface scattering work, both 2-D and 3-D, are on-going efforts done in collaboration with Dr. Mohsen Badiey and his colleagues at the Univ. of Delaware. This work is expected to continue in FY12. The work on 3-D effects of nonlinear internal waves was an FY10-11 effort done in collaboration with Dr. James Miller and his colleagues at the Univ. of Rhode Island. The scattered vector field work was done in collaboration with Dr. Bob Barton and his colleagues at the Naval Undersea Warfare Center, Newport. This work is expected to continue in FY12 with other funding, and will begin to coordinate efforts with colleagues at APL-UW.

REFERENCES

1. Smith, K.B., "Convergence, stability, and variability of shallow water acoustic predictions using a split-step Fourier parabolic equation model," J. Comp. Acoust., Vol. 9, pp. 243-285, 2001.
2. Tappert, F.D. and Nghiem-Phu, L., "A new split-step Fourier algorithm for solving the parabolic wave equation with rough surface scattering," J. Acoust. Soc. Am. 77, S101, 1985.
3. Thomson, D.J. and Chapman, N.R., "A wide angle split-step algorithm for the parabolic equation," J. Acoust. Soc. Am. 74, pp. 1848-1854, 1983.

PUBLICATIONS

1. Senne, J., Song, A., Badiey, M, and Smith, K.B., "Parabolic equation modeling of high frequency acoustic transmission with an evolving sea surface," J. Acoust. Soc. Am., 2011 [submitted].
2. Dossot, G.A., Badiey, M., Smith, K.B., Miller, J.H., Potty, G.R., and Lynch, J.F., "Evidence of escalating acoustic intensity preceding a strong internal wave event during the Shallow Water '06 experiment," J. Acoust. Soc. Am., 2011 [submitted].
3. Barton, R.J., Smith, K.B., and Vincent, H.T., "A characterization of the scattered acoustic intensity field in the resonance region for simple spheres," J. Acoust. Soc. Am. 129, pp. 2772-2784, 2011.
4. Smith, K.B., Badiey, M., and Senne, J., "Three-dimensional surface scattering using a parabolic equation model," J. Acoust. Soc. Am., 2011 [submitted].
5. Barton, R.J., Moss, G.R., and Smith, K.B., "Characterization of scattered acoustic intensity fields of finite cylinders in the resonance region," J. Acoust. Soc. Am., 2011 [submitted].

6. Song, A., Senne, J.M., Badiey, M., and Smith, K.B., “Underwater acoustic communication channel simulation using parabolic equation,” J. Acoust. Soc. Am., 2011 [submitted].

7. Senne, J.M., Song, A., Smith, K., and Badiey, M., “An investigation of the effects of rough seas and bubble injections on high frequency propagation using a parabolic equation method,” J. Acoust. Soc. Am., 2011 [submitted].

8. Barton, R.J., Dossot, G.A., and Smith, K.B., “Variations in the active and reactive intensity components of the sound field due to nonlinear internal waves,” J. Acoust. Soc. Am., 2011 [submitted].

9. Dossot, G.A., Miller, J.H., Potty, G.R., Smith, K.B., Badiey, M., and Lynch, J.F., “Three dimensional parabolic equation modeling of acoustic intensity fluctuations due to internal wave phenomena,” J. Acoust. Soc. Am. 129, pp. 2457, 2011.

10. Dossot, G.A., Miller, J.H., Potty, G.R., Smith, K.B., Lynch, J.F., Lin, Y.-T., Newhall, A.E., and Badiey, M., “Simulating Acoustic Pressure and Intensity in a Strong Internal Wave Field,” Proceedings of 10th International Conference on Theoretical and Computational Acoustics, Taipei, Taiwan, 25-28 April, 2011.

11. Barton, R.J. and Smith, K.B., “A Characterization of Scattered Acoustic Intensity Vector Fields in the Resonance Region,” Proceedings of 10th International Conference on Theoretical and Computational Acoustics, Taipei, Taiwan, 25-28 April, 2011.